The Effects of Site-Directed Mutagenesis on Hemerythrin-like Protein Rv2633c

2018

Kelly M. Rosch
University of Central Florida

THE EFFECTS OF SITE-DIRECTED MUTAGENESIS ON HEMERYTHRIN-LIKE PROTEIN Rv2633c

by

KELLY M. ROSCH

A thesis submitted in partial fulfillment of the requirements

For the Honors in the Major Program in Biomedical Sciences

In the College of Medicine and in the Burnett Honors College

At the University of Central Florida

Fall Term, 2018

Thesis Chair: William T. Self, Ph.D.

Abstract

Mycobacterium tuberculosis (*Mtb*) is the causative agent of tuberculosis, one of the top ten causes of death worldwide. One of the genes upregulated in *Mtb* during macrophage infection is *rv2633c*, but the structure and function of its gene product remain unknown. Preliminary research has indicated that Rv2633c is a hemerythrin-like protein that exhibits catalase activity and binds two iron atoms using an HHE domain. Additionally, Rv2633c appears to exist as a dimer. The purpose of this project is to identify specific residues outside of the HHE domain that contribute to the protein's iron-binding ability and/or catalase activity, and to determine whether residues on the C terminus are required for dimerization. Conserved residues D37, E42, and E95 were selected due to their proximity in the amino acid sequence to the HHE domain. Each residue was mutated to alanine using site-directed mutagenesis and the mutations were confirmed using Sanger sequencing. The E95A mutant and the C-terminal truncation mutant were expressed in *Escherichia coli* using the T7 expression system and purified using affinity chromatography. While wild-type Rv2633c eluted as a soluble protein, the C-terminal truncation mutant was not soluble, indicating that the C terminus may be required for Rv2633c folding. The E95A mutant eluted as a soluble protein, but may have lower iron content than wild-type Rv2633c, indicating that this glutamic acid residue could contribute to iron-binding, despite being outside the HHE domain.

Acknowledgments

Heartfelt thanks to my thesis committee, Dr. William Self, Dr. Sean Moore, Dr. Kyle Rohde, and Dr. Kenneth Teter, for their guidance, and to Michael Johnstone and Kyle Strickland for the good times.

TABLE OF CONTENTS

List of Figures

INTRODUCTION

Mycobacterium tuberculosis

Mycobacterium tuberculosis (*Mtb*) is a rod-shaped species of bacteria that causes tuberculosis disease (TB). TB is one of the top ten causes of death worldwide, killing 1.3 million people in 2017, and latently infecting one fourth of the world's population [1]. Despite research efforts dating back to the 19th century, a highly effective vaccine for *Mtb* has not been developed [1]. TB is a health concern in developing countries, with 60% of cases originating in India, Indonesia, China, Nigeria, Pakistan, and South Africa [1]. A significant challenge in eradicating TB remains the discrepancy between the predicted number of cases that occur and the number of cases that are diagnosed and reported.

TB is spread through the air through coughing, sneezing, and speaking. Droplet nuclei containing *Mtb* enter the upper respiratory system, and are cleared in most cases before reaching the lower respiratory system. If *Mtb* does reach the lung mucosa, it is engulfed by resident macrophages through phagocytosis and becomes enclosed in the phagosome. Typically, the phagosome fuses with the lysosome, a harsh intracellular compartment with low pH. When these two compartments fuse, they form the phagolysosome, which degrades the bacteria within. However, *Mtb* is able to prevent fusion of the phagosome to the lysosome [2]. This ability allows *Mtb* to replicate inside host macrophages.

Oxidative Stress in *Mtb*

One way that *Mtb* may have evolved to survive inside the macrophage is through resisting oxidative stress [3]. Oxidative stress is caused by reactive oxygen species produced during the immune response such as superoxide (O_2-), peroxide (H_2O_2),

hypochlorite (HClO), hydroxyl radicals, and peroxynitrite (ONOO-) [3]. These reactive oxygen and nitrogen species damage bacterial DNA, proteins, and lipids. A common bacterial defense against reactive oxygen species is the catalase class of enzymes, which converts peroxide into water and oxygen [3]. *Mtb* contains a well-studied catalase, KatG, which neutralizes the peroxides generated by NADPH oxidase [4].

Hemerythrin-like proteins

Contrary to their name, hemerythrin-like proteins do not contain heme. Instead, hemerythrin-like proteins are characterized by the presence of an HHE domain, which consists of two histidine residues and a glutamic acid residue, often distributed over two separate alpha helices [5, 6]. The HHE domain in hemerythrin-like proteins commonly binds two iron atoms [7, 8]. Hemerythrin-like proteins typically bind oxygen, and are present in a wide variety of bacteria. Some hemerythrin-like proteins contain additional signal transduction domains, indicating that these proteins play diverse roles [9].

Rv2633c

Rv2633c is a gene found in *Mtb* that is upregulated as *Mtb* infects the macrophage [10, 11]. Additionally, *rv2633c* is upregulated *in vitro* when *Mtb* is grown in acidic conditions [12]. Species of *Mycobacteria* that contain the *rv2633c* gene tend to be more pathogenic, indicating that *rv2633c* may contribute to virulence [13]. Furthermore, when *rv2633c* is inactivated by a transposon insertion, *Mtb* is attenuated when injected into the tail vein of a mouse model [14]. Previous research has shown that Rv2633c exhibits catalase activity with a k_{cat} of 1475 s^{-1} and a K_m of 10.1±1.7 mM [13]. Together, these studies indicate that Rv2633c may contribute to *Mtb* pathogenicity by combating reactive oxygen species within the macrophage.

While the structure of Rv2633c remains unknown, it contains an HHE domain, and has been shown to bind two iron atoms in a manner consistent with other Hemerythrin-like proteins [13]. However, unlike hemerythrin-like proteins, Rv2633c exhibits catalase activity instead of reversibly binding oxygen. Furthermore, while hemerythrin-like proteins commonly form octamers, Rv2633c has been shown to migrate through a size-exclusion column as a dimer [13]. The unique combination of an HHE domain and catalase activity in Rv2633c makes this protein the first example of a non-heme di-iron catalase.

The purpose of this project is to identify specific residues outside of the HHE domain that contribute to the protein's iron-binding ability and catalase activity, and to determine whether residues on the C terminus are required for the dimerization of Rv2633c.

MATERIALS AND METHODS

Design of Rv2633c Mutants

To determine residues outside of the HHE domain that affect iron-binding in Rv2633c, highly conserved residues were chosen based on their proximity to the HHE domain in the primary amino acid sequence of Rv2633c. Based on this method, residues D37, E42, and E95 were chosen for mutation. Each residue was mutated to alanine, because aspartic acid (D) and glutamic acid (E) are highly charged, whereas alanine is neutral. This mutation preserves the structure of the protein while eliminating any functionality due to the charge of the amino acid side chain.

To determine whether the C terminus of Rv2633c is necessary for dimerization of the protein, a C-terminal truncation mutant was constructed. The exact residues to delete were determined by analyzing the SWISS-MODEL predicted structure of Rv2633c. The predicted structure consisted of four alpha helices arranged in a barrel shape around a di-iron center, with a fifth alpha helix positioned away from the barrel on the C-terminal end. The C-terminal truncation mutant was generated by deleting this fifth alpha helix, corresponding to residues I122-I161. The 6XHis tag and stop codon were moved to the end of the fourth alpha helix, thus shortening Rv2633c.

Construction of Rv2633c Mutants

A pET23a vector was used for cloning and generation of Rv2633c mutants. Each point mutant was generated using ‘Round the Horn mutagenesis, a polymerase chain reaction (PCR) based technique [15]. This method entailed designing a forward primer that annealed immediately downstream of the mutation site, and a reverse primer that contained the desired mutation. The C-terminal truncation (ΔI122-I161) mutant was

generated by designing a forward primer that annealed to the 6XHis tag and stop codon, and a reverse primer that annealed to the last amino acid in the fourth alpha helix. This primer placement ensured that the DNA between the forward and reverse primers was deleted, removing residues I122-I161 from the C-terminal end of Rv2633c.

Prior to performing PCR, each forward and reverse primer was phosphorylated using PNK, 100 mM ATP, and 10X PNK buffer. This step is necessary for the ligation of the linear PCR product because restriction enzymes are not used in 'Round the Horn mutagenesis.

After phosphorylating each primer, PCR was performed to introduce each desired mutation and amplify the mutant DNA. Each PCR was conducted with 25 μL deionized water, 10 μL 5X Q5 buffer, 10 μL GC enhancer, 1.5 μL phosphorylated forward and reverse primers, 1 μL 10 mM dNTPs, 40 ng plasmid template, and 0.5 μL Q5 DNA polymerase. The reaction was heated to 98°C for one minute, 96°C for 30 seconds, 60°C for 30 seconds, and 72°C for 2.5 minutes. This cycle was repeated 28 times before cooling to 18°C.

Success of the PCR was determined by 0.8% agarose gel electrophoresis. Each well was loaded with 5 μL PCR product and 2 μL 6X loading buffer. The gel was submerged in 1X Tris-Acetate EDTA buffer and run at constant volts (100 V) for 30 minutes. The gel was imaged using ultraviolet light. Presence of a 4 kb band indicated PCR success.

Confirmation of Rv2633c Mutants

Mutant PCR products were purified using crystal violet agarose gel extraction. Each purified linear PCR product was ligated to form circular DNA by incubating 4 μL

PCR product with 4.6 μL deionized water, 1 μL 10X T4 DNA ligase buffer, and 0.4 μL T4 DNA ligase. The reaction was incubated at room temperature for 10 minutes.

The ligated PCR product was transformed into NEB 5-alpha *E. coli* using the NEB protocol for heat shock transformation. Transformed cells were plated on LB-Lennox agar supplemented 100 μg/mL ampicillin to select for cells containing the pET23a plasmid.

Plasmids containing Rv2633c mutants were prepared for sequencing by alkaline lysis (miniprep). A 10 μL solution of 50% plasmid in deionized water was shipped to GeneWiz for Sanger sequencing.

Purification of Rv2633c Mutants

Each verified mutant was transformed into Lemo21(DE3) (New England Biolabs) using the protocol provided for heat shock transformation. Transformed cells were plated on LB-Lennox supplemented with 0.2% glucose, 0.2% glycerol, and 200 μg/mL ampicillin. The presence of glucose at this concentration prevented the premature expression of mutant Rv2633c. Glycerol served as a carbon source and alternative to the amino acids supplied by the tryptone in LB-Lennox. Ampicillin was used to select for cells containing the pET23a plasmid, but in this case, the concentration of ampicillin was doubled to ensure that the plasmid is not lost prior to expression and purification. Serial dilutions of transformed NEB Lemo21(DE3) were plated with 100 μg/mL ampicillin and 200 μg/mL ampicillin, and no noticeable growth difference was observed.

Each mutant was grown at 37°C for 12-16 hours in a liquid culture of LB-Lennox supplemented with 0.2% glucose, 0.2% glycerol, 1 mM magnesium sulfate, and 200 μg/mL ampicillin. The liquid culture was diluted 1:100 in LB-Lennox supplemented with

0.2% glycerol, 1 mM magnesium sulfate, and 200 μg/mL ampicillin. Glucose was excluded from the media during this stage to allow for maximum expression of mutant Rv2633c using the T7 expression system.

After 1.5 hours, the temperature of the incubator was reduced to 18°C to assist in folding of mutant Rv2633c. When the temperature reached 18°C, expression of mutant Rv2633c was induced with 1 mM IPTG. 500 mg/L Mohr's salt was added to allow formation of the iron cofactor. The culture was incubated at 18°C for 7 hours and harvested immediately after this period by centrifugation at 12,000 x g for 10 minutes at 4°C. Each cell pellet was resuspended in cell wash buffer containing 25 mM Tris and 1 mM EDTA, and centrifuged again at the same specifications.

The washed cell pellet was resuspended in 5 mL lysis buffer containing 25 mM Tris and 1 mM benzamidine. Lysozyme was added to a concentration of 1 mM, and this mixture was placed on a rotator for 30 minutes at 4°C. To aid in lysis, chloroform was added at a final concentration of 10 μL/mL lysate. 0.25 μL Pierce Universal Nuclease was added to degrade genomic DNA. The resulting lysate was centrifuged at 28,000 x g for 20 minutes at 4°C to separate soluble protein from insoluble protein.

Cobalt affinity column resin was prepared by centrifugation at 1,000 x g for 5 minutes at 4°C. Damaged beads were removed by decanting the supernatant. Soluble lysate was added to 2 mL of cobalt resin and placed on a rotator for 30 minutes at 4°C.

Unbound protein was collected by adding the soluble lysate and cobalt resin to a gravity column and allowing the liquid phase to pass through the column. The column was washed with 3 column volumes (6 mL) of wash buffer containing 25 mM Tris and 15 mM imidazole. Each wash was collected in a separate conical tube. Bound protein was

eluted using one column volume of elution buffer containing 25 mM Tris and 300 mM imidazole.

The protein content of the pre-induction cells, post-induction cells, total lysate, insoluble lysate, soluble lysate, unbound, wash, and elution samples was determined using 12% SDS-PAGE. Each SDS-PAGE gel was submerged in 1X Tris-Glycine buffer and run at constant amps (135 A) for 30-45 minutes. Gels were stained using GelCode Blue and destained using 10% acetic acid. Elution samples with the highest concentration of Rv2633c were pooled, and residual imidazole was removed by dialysis into 20 mM HEPPS, a HEPES-based buffer.

Determination of Mutant Rv2633c Iron Content

The iron content of mutant Rv2633c was determined by UV-vis absorbance spectrum analysis. The spectrophotometer was blanked using 60 μL 20 mM HEPPS. The UV absorbance of each Rv2633c sample was measured from 250 nm to 700 nm. Three samples of dialyzed Rv2633c from each purification were measured and the absorbance at each wavelength was averaged. The resulting absorbances were graphed in Prism.

RESULTS

Figure 1: Coordination of iron atoms by HHE domain in hemerythrin-like proteins

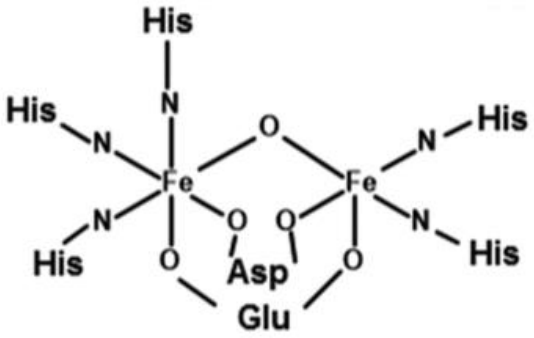

The HHE domain of hemerythrin-like proteins commonly coordinates two iron atoms, as shown above in a previously reported model [13]. Specifically, the iron atoms are coordinated by the side chains of histidine, aspartic acid, and glutamic acid residues. Previous research has shown that mutations in residues within the HHE domain result in loss of the iron cofactor in Rv2633c.

Figure 2: Location of point mutations and truncation mutation relative to the HHE domain in Rv2633c

```
          10         20         30         40         50
MNAYDVLKRH HTVLKGLGRK VGEAPVNSEE RHVLFDEMLI ELDIHFRIED
          60         70         80         90        100
DLYYPALSAA GKPITGTHAE HRQVVDQLAT LLRTPQRAPG YEEEWNVFRT
         110        120        130        140        150
VLEAHADVEE RDMIPAPTPV HITDAELEEL GDKMAARIEQ LRGSPLYTLR
         160
TKGKADLLKA I
```

Highly conserved, charged amino acids were selected for mutation based on their proximity to the HHE domain in the sequence of Rv2633c. Here, the HHE domain is shown in yellow and the amino acids selected for mutation are shown in red. The deleted

region of the truncation mutant is also shown in red at the C-terminal end of the amino acid sequence.

Figure 3: SWISS-MODEL Rv2633c structure prediction

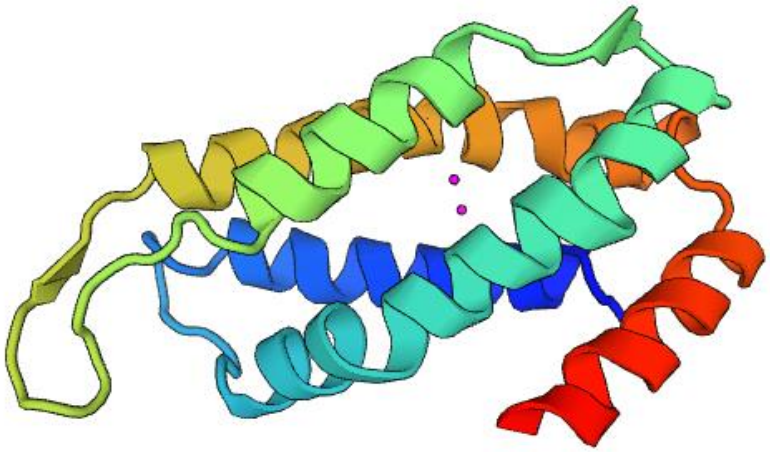

Because the structure of Rv2633c remains unknown, SWISS-MODEL was used to generate a predicted structure. Hypothetical protein NMB1532 from *Neisseria meningitidis* was algorithmically chosen by SWISS-MODEL to serve as the structural template for Rv2633c. Based on the structure of NMB1532, Rv2633c was predicted to contain four alpha helices arranged in a barrel shape around the di-iron cofactor, shown as two pink circles inside the barrel, with a fifth alpha helix on the C-terminal end of Rv2633c positioned outside the barrel. For clarity, this helix is shown in red. This predicted structure led to the hypothesis that the fifth alpha helix is involved in dimerization. The C-terminal truncation mutant lacks this fifth alpha helix, corresponding to residues I122-I161.

Figure 4: Approximate locations of Rv2633c point mutations based on homology to NMB1532

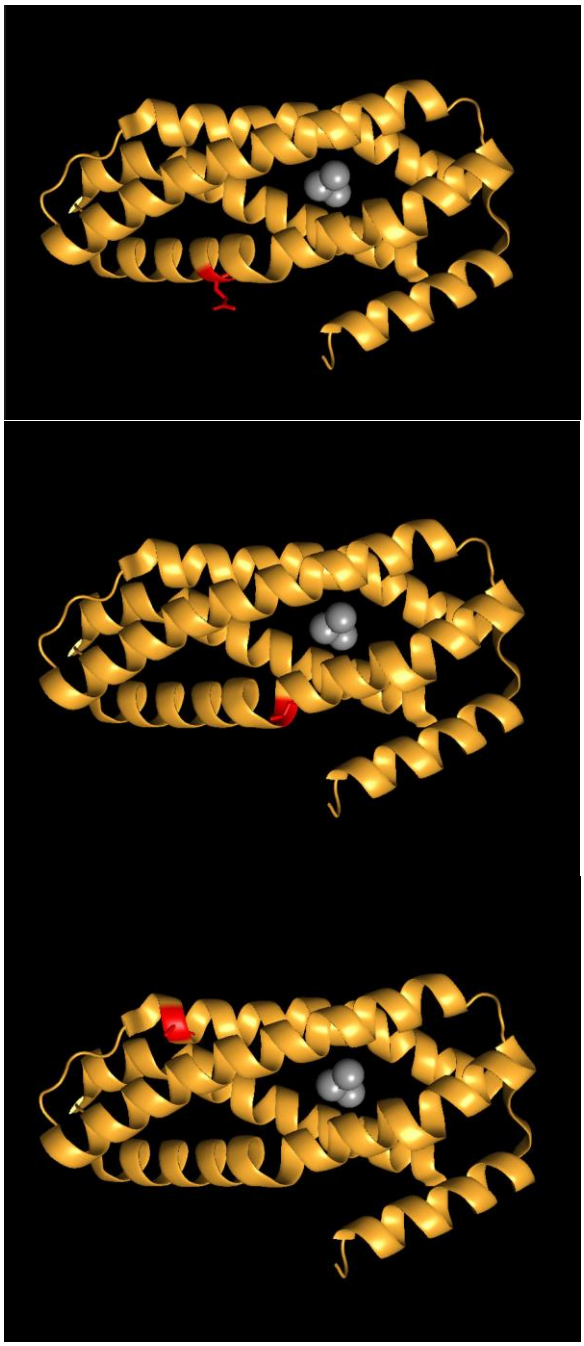

From top, the approximate locations of Rv2633c mutations D37A, E42A, and E95A are shown based on the structure of NMB1532, a protein projected by SWISS-MODEL to be structurally similar to Rv2633c. While these locations are only

approximate, they serve as a rough indicator of the proximity of each mutant amino acid to the iron cofactor in Rv2633c. It should be noted that the original plan for mutagenesis was based solely on the primary amino acid sequence and alignments with similar HHE domain proteins, and not on this modeled structure.

Figure 5: Approximation of Rv2633c C-terminal truncation mutant based on homology to NMB1532

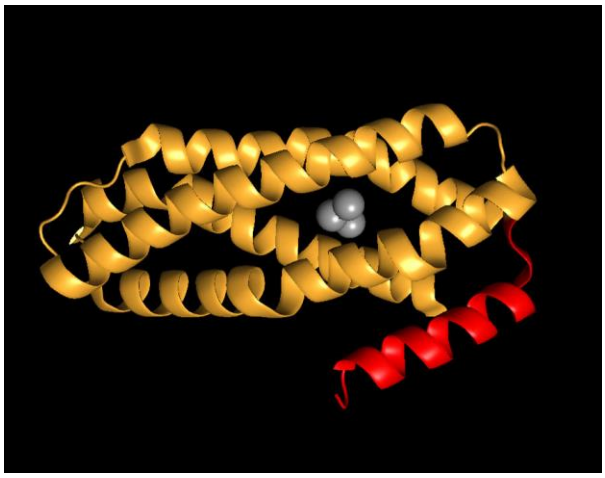

The approximate portion of Rv2633c that is deleted in the ΔI122-I161 mutant is modeled here, again using the structure of NMB1532 as a template. The purpose of creating this mutant is to determine whether the predicted C-terminal alpha helix is necessary for dimerization in Rv2633c.

Figure 6: Successful generation of D37A and E42A Rv2633c PCR products

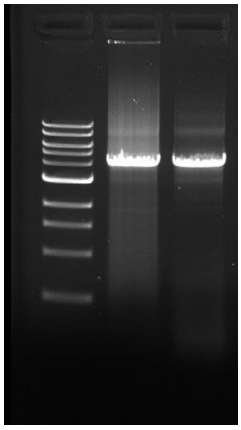

D37A and E42A Rv2633c mutant PCR products were visualized using a 0.8% agarose gel to confirm successful PCR. From left, lane 1 contained 7 μL Tri-dye ladder; lane 2 contained 5 μL D37A PCR product and 2 μL 6X DNA loading buffer; lane 3 contained 5 μL E42A PCR product and 2 μL 6X DNA loading buffer. Both D37A and E42A PCR products appeared as bands at approximately 4 kb, indicating successful PCR.

Figure 7: Successful generation of E95A Rv2633c PCR product

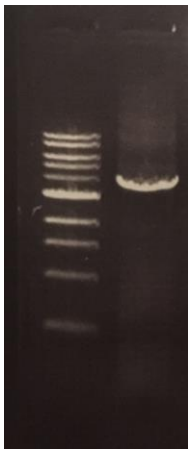

E95A Rv2633c mutant PCR product was visualized using a 0.8% agarose gel to confirm successful PCR. From left, lane 1 contained 7 μL Tri-dye ladder, and lane 2

contained 5 μL E97A PCR product and 2 μL 6X DNA loading buffer. E95A PCR product appeared as a band at approximately 4 kb, indicating successful PCR.

Figure 8: Successful generation of ΔI122-I161 Rv2633c PCR product

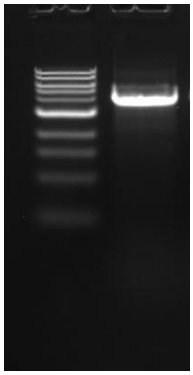

ΔI122-I161 mutant Rv2633c PCR product was visualized using a 0.8% agarose gel to confirm successful PCR. From left, lane 1 contained 7 μL Tri-dye ladder, and lane 2 contained 5 μL ΔI122-I161 PCR product and 2 μL 6X DNA loading buffer. ΔI122-I161 PCR product appeared as a band at approximately 4 kb, indicating successful PCR.

Figure 9: Expression and native purification of wild-type Rv2633c

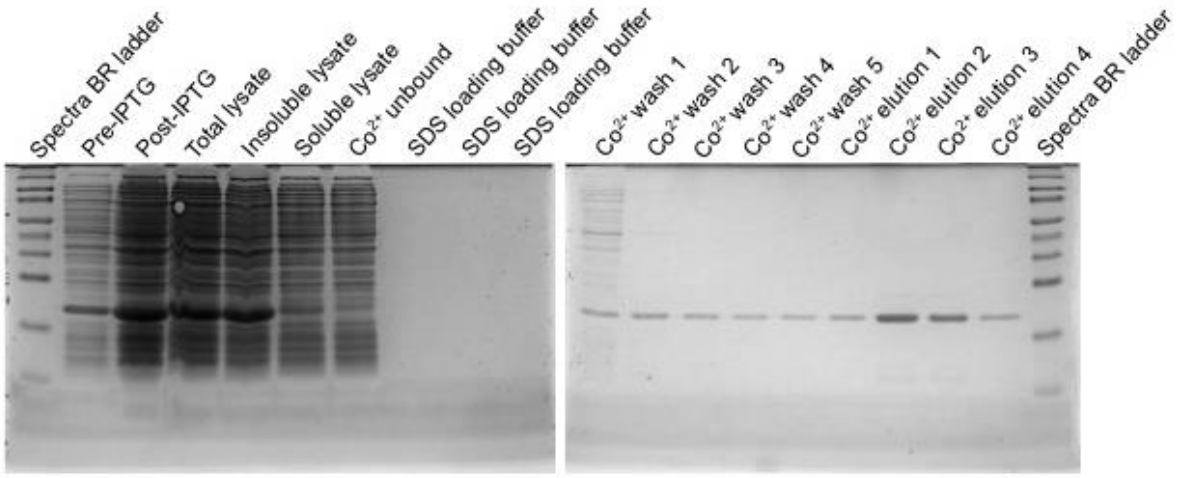

Wild-type Rv2633c was expressed and purified using cobalt affinity chromatography. Each step of the purification was visualized using 12% SDS-PAGE to assess purity and solubility of eluted wild-type Rv2633c. Consistent with previous reports, wild-type Rv2633c eluted as a soluble 18 kDa protein. Lanes 2-7 on the left gel and lanes 1-9 on the right gel were loaded with 5 μL from a mixture of 8 μL sample and 32 μL SDS loading buffer. Lanes 8-10 on the left gel were loaded with 5 μL SDS loading buffer to prevent uneven migration of bands through the gel. Slight contamination is visible in elution samples 2 and 3, but did not noticeably affect the absorbance spectrum (Figure 12).

Figure 10: Expression and native purification of E95A Rv2633c

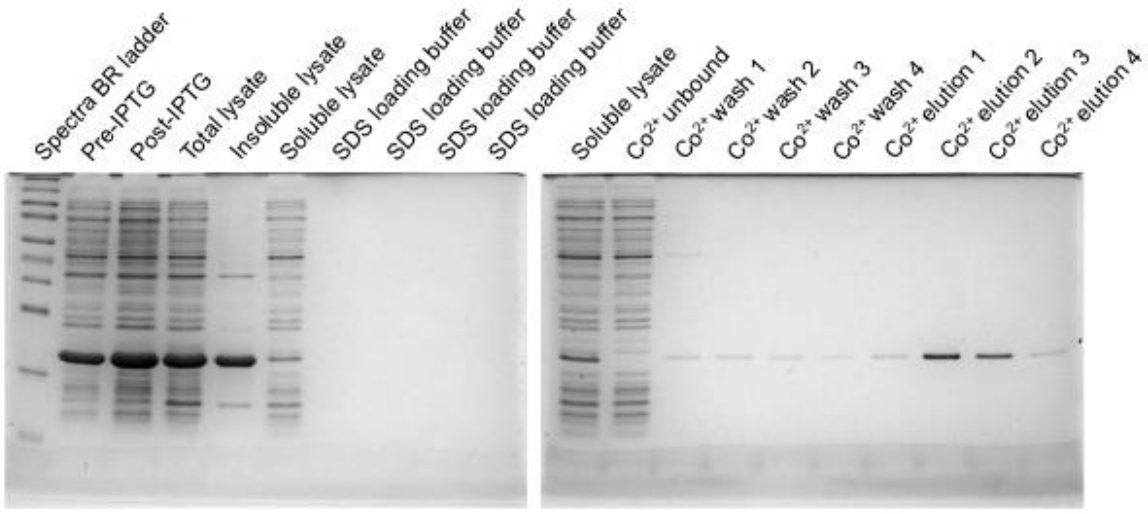

E95A Rv2633c was expressed and purified using cobalt affinity chromatography, using the same protocol as the purification of wild-type Rv2633c (Figure 9). Each step of the purification was visualized using 12% SDS-PAGE to assess purity and solubility of eluted E95A Rv2633c. Similar to wild-type Rv2633c, E95A Rv2633c eluted as a soluble 18 kDa protein. Lanes 2-6 on the left gel and lanes 1-10 on the right gel were loaded with 5 μL from a mixture of 8 μL sample and 32 μL SDS loading buffer. Lane 1 on the left gel was loaded with 5 μL pre-stained Spectra Broad-Range protein ladder. E95A soluble lysate was used as a ladder on the right gel. Lanes 7-10 on the left gel were loaded with 5 μL SDS loading buffer to prevent uneven migration of bands through the gel. No contaminants were visible in the elution lanes, even after magnification of a high-resolution image.

Figure 11: ΔI122-I161 Rv2633c did not elute as a soluble protein

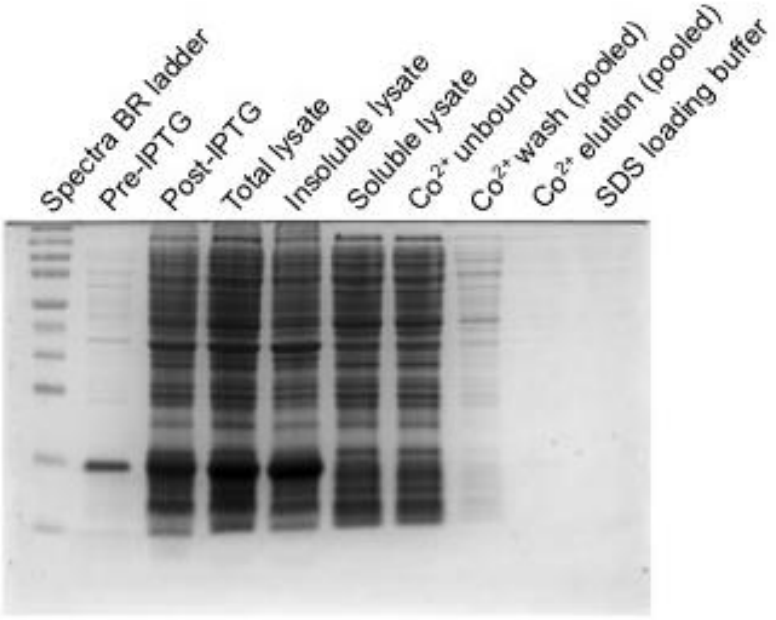

ΔI122-I161 Rv2633c was expressed and purified using cobalt affinity chromatography, using the same protocol as the purification of wild-type and E95A Rv2633c (Figures 9, 10). However, unlike wild-type and E95A Rv2633c, ΔI122-I161 Rv2633c did not elute as a soluble protein. From left, lanes 2-9 were loaded with 6 μL from a mixture of 8 μL sample and 32 μL SDS loading buffer. Lane 1 was loaded with 6 μL pre-stained Spectra Broad Range protein ladder. Lane 10 was loaded with 6 μL SDS loading buffer to prevent uneven migration of bands through the gel.

The lack of soluble ΔI122-I161 Rv2633c may be due to aggregation or misfolding caused by the C-terminal deletion. While SWISS-MODEL predicted that the deleted region of Rv2633c was positioned separately from the rest of the protein, it is possible that this model is incorrect. The ΔI122-I161 mutation may have disrupted the overall structure of Rv2633c, leading to aggregation or misfolding.

Figure 12: Rv2633c exhibited varying iron content based on UV-vis spectra

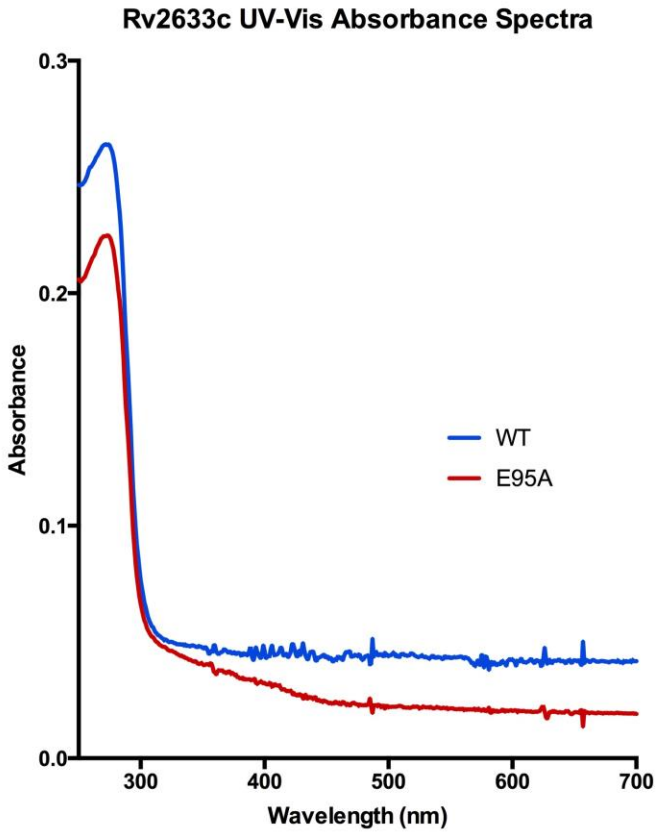

The UV-vis spectrum of E95A was analyzed and compared to the spectrum of wild-type Rv2633c to determine iron content. Each purified Rv2633c was dialyzed into 20 mM HEPPS to remove residual imidazole before spectral analysis. Presence of the iron cofactor was indicated by a broad absorbance from 300-360 nm. While wild-type Rv2633c normally exhibits this absorbance pattern, this preparation of wild-type Rv2633c did not. Previous attempts to purify Rv2633c indicate that the iron content is inconsistent, even between replicates using the same purification protocol. E95A Rv2633c may contain iron, but possibly not to the same degree as wild-type Rv2633c typically does (Figure 13). However, due to the inconsistent nature of iron content in

Rv2633c, it is difficult to draw conclusions about the iron content of the E95A mutant based on a single preparation.

Figure 13: Rv2633c previously exhibited a broad absorbance indicative of iron content

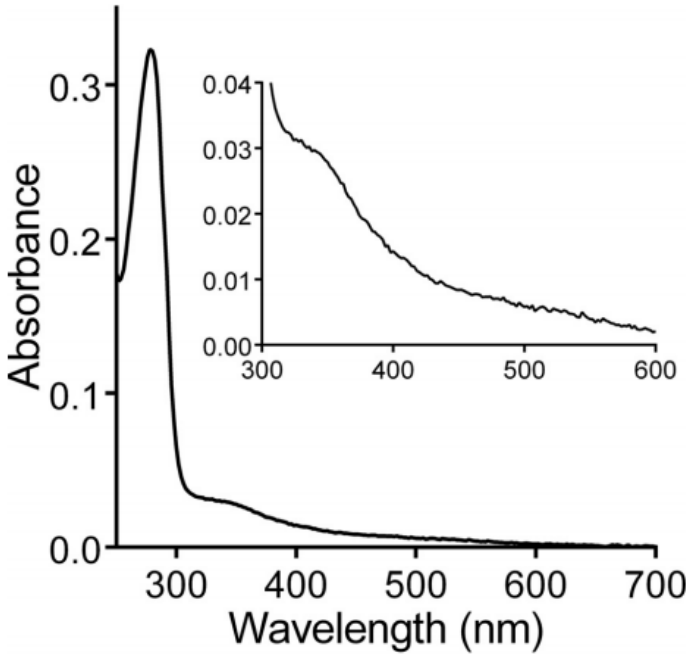

As reported in 2017, wild-type Rv2633c typically exhibits a broad absorbance from 300-360 nm, which is indicative of the iron cofactor in a hemerythrin-like protein [13]. While E95A Rv2633c exhibited a similar absorbance pattern, it was between 300 and 450 nm instead of the characteristic 300-360 nm absorbance pattern shown above. The lengthened absorbance in this preparation of E95A Rv2633c may be due to cobalt resin that passed through the base of the gravity column during elution.

DISCUSSION

Based on the finding that wild-type Rv2633c elutes as a soluble protein (figure 9), it is interesting that the C-terminal truncation mutant is not soluble (figure 10). This difference may indicate that the deleted region of amino acids at the C terminus leads to aggregation or improper folding of Rv2633c. This region was projected by SWISS-MODEL to fold into a discrete alpha helix, separate from the rest of the protein, but it is possible that this projection is inaccurate. The degree of homology between Rv2633c and NMB1532, the protein used to generate the predicted structure of Rv2633c, is only 18%, so it is not surprising that this model of Rv2633c structure may be inaccurate.

Perhaps the structure of Rv2633c more closely resembles Ytfe, an iron-sulfur cluster repair protein that SWISS-MODEL determined had the second-highest level of structural homology to Rv2633c. When Ytfe is used as the structural template for Rv2633c, only four alpha helices are present instead of five. The C-terminal truncation would then delete part of the fourth alpha helix, interfering with the symmetry of the protein as a whole. Further replicates of purification may be necessary to confirm that the deleted section of the C-terminus is indeed required for folding in Rv2633c. While this is an interesting finding, it does not answer the original question of whether the C-terminus is involved in dimerization. This question may be answered by deleting fewer amino acids from the C-terminal end of Rv2633c, because this new construct may be less likely to aggregate or misfold.

The point mutation E95A eluted as a soluble protein, which was expected because the point mutation was unlikely to cause major structural changes in Rv2633c. Past experiments have shown that even when a point mutation causes Rv2633c to lose its iron

cofactor, Rv2633c is still soluble. However, it is surprising that the UV-vis spectra in this study differ in iron content from the previously reported UV-vis spectrum of wild-type Rv2633c. Previous attempts at Rv2633c purification indicate that the iron content fluctuates drastically between purifications, even when identical protocols are used. This indicates that the findings in this study may not represent an accurate picture of Rv2633c iron content, since each mutant was only purified once. Despite this uncertainty, it is promising that the E95A mutant appears to contain less iron cofactor than the previously reported iron content of wild-type Rv2633c. This may indicate that residue E95 is involved in stabilization of the iron cofactor, despite being outside the HHE domain that normally coordinates iron.

In addition to establishing the iron content of E95A Rv2633c, further studies may analyze this mutant's catalase activity. The variability in iron content and in protein stability has proven difficult in both wild type and mutant forms of the protein. Ideal protein expression conditions and purification is an ongoing part of the research with this family of proteins.

As a whole, these results contribute to further biochemical characterization of Rv2633c, the first example of a non-heme di-iron catalase. Further research about the regulation and behavior of this protein is important in order to understand how *Mtb* thrives inside the macrophage. Research in this area may reverse the trend of multi-drug resistant TB and develop an effective vaccine.

Literature Cited

1. World Health Organization. (2018). Global tuberculosis report 2018.

2. Rohde, K. H., Veiga, D. F., Caldwell, S., Balázsi, G., & Russell, D. G. (2012). Linking the transcriptional profiles and the physiological states of Mycobacterium tuberculosis during an extended intracellular infection. *PLoS pathogens*, *8*(6), e1002769.

3. Nambi, S., Long, J. E., Mishra, B. B., Baker, R., Murphy, K. C., Olive, A. J., ... & Sassetti, C. M. (2015). The oxidative stress network of Mycobacterium tuberculosis reveals coordination between radical detoxification systems. *Cell host & microbe*, *17*(6), 829-837.

4. Ng, V. H., Cox, J. S., Sousa, A. O., MacMicking, J. D., & McKinney, J. D. (2004). Role of KatG catalase-peroxidase in mycobacterial pathogenesis: countering the phagocyte oxidative burst. *Molecular Microbiology*, *52*(5), 1291-1302.

5. Takagi, T., & Cox, J. A. (1991). Primary structure of myohemerythrin from the annelid Nereis diversicolor. *FEBS letters*, *285*(1), 25-27.

6. Karlsen, O. A., Ramsevik, L., Bruseth, L. J., Larsen, Ø., Brenner, A., Berven, F. S., ... & Lillehaug, J. R. (2005). Characterization of a prokaryotic haemerythrin from the methanotrophic bacterium *Methylococcus capsulatus* (Bath). *The FEBS Journal*, *272*(10), 2428-2440.

7. Stenkamp, R. E. (1994) Dioxygen and hemerythrin. Chem. Rev. 94, 715–726

8. Holmes, M. A., Le Trong, I., Turley, S., Sieker, L. C., & Stenkamp, R. E. (1991). Structures of deoxy and oxy hemerythrin at 2.0 Å resolution. *Journal of molecular biology*, *218*(3), 583-593.

9. French, C. E., Bell, J. M., & Ward, F. B. (2007). Diversity and distribution of hemerythrin-like proteins in prokaryotes. *FEMS microbiology letters*, *279*(2), 131-145.

10. Rohde, K. H., Abramovitch, R. B., and Russell, D. G. (2007) Mycobacterium tuberculosis invasion of macrophages: linking bacterial gene expression to environmental cues. Cell Host Microbe 2, 352–364

11. Homolka, S., Niemann, S., Russell, D. G., and Rohde, K. H. (2010) Functional genetic diversity among *Mycobacterium tuberculosis* complex clinical isolates: delineation of conserved core and lineage-specific transcriptomes during intracellular survival. PLoS Pathog. 6, e1000988

12. Abramovitch, R. B., Rohde, K. H., Hsu, F.-F., and Russell, D. G. (2011) aprABC:A *Mycobacterium tuberculosis* complex-specific locus that modulates pH-driven adaptation to the macrophage phagosome. Mol. Microbiol. 80, 678–694.

13. Ma, Z., Strickland, K. T., Cherne, M. D., Sehanobish, E., Rohde, K. H., Self, W. T., & Davidson, V. L. (2018). The Rv2633c protein of Mycobacterium tuberculosis is a non-heme di-iron catalase with a possible role in defenses against oxidative stress. *Journal of Biological Chemistry*, *293*(5), 1590-1595.

14. Sassetti, C. M., and Rubin, E. J. (2003) Genetic requirements for mycobacterial survival during infection. Proc. Natl. Acad. Sci. U.S.A. 100, 12989–12994.

15. Moore, S. (n.d.). 'Round-the-horn site-directed mutagenesis. Retrieved March 02, 2018, from https://openwetware.org/wiki/%27Round-the-horn_site-directed_mutagenesis